Evaluation of pulse width modulation techniques to reduce total harmonic distortion in grid-connected PV systems

Bouledroua Adel, Mesbah Tarek, Kelaiaia Samia
Department of Electrical Engineering, Faculty of Technology, Badji Mokhtar University, Annaba, Algeria

Article Info

ABSTRACT

The proliferation of grid-connected photovoltaic systems (GCPVs) has created significant challenges in maintaining power quality standards, particularly with respect to total harmonic distortion (THD). This research is concerned with evaluating three well-known pulse width modulation (PWM) techniques - sine PWM (SPWM), third harmonic injection PWM (THIPWM), and space vector PWM (SVPWM) for their effectiveness in mitigating THD in three-phase single-stage GCPVs. Through extensive simulations performed in MATLAB/Simulink, a comprehensive comparative analysis is presented that reveals the strengths and limitations of each PWM strategy. The results show that SVPWM is the most effective technique for THD mitigation and outperforms its counterparts. THIPWM proves to be a promising second-best option, while SPWM lags behind in terms of harmonic suppression capabilities. This research not only quantifies the THD reduction achieved by each PWM technique but also delves into the underlying mechanisms and theoretical underpinnings that contribute to their distinct performances. The results are further supported by detailed harmonic spectrum analyses, providing valuable insights into the harmonic profiles associated with each modulation strategy.

Corresponding Author:

Bouledroua Adel
Department of Electrical Engineering, Faculty of Technology, Badji Mokhtar University
Annaba 23000, Algeria
Email: adel.bouledroua@univ-annaba.dz

1. INTRODUCTION

Grid-connected photovoltaic systems (GCPVs) have recently gained considerable attention as promising alternative and viable energy sources among the existing renewable energies to fulfill the ever-growing global energy demand [1], [2]. However, GCPV integration often undergoes power quality (PQ) issues, particularly total harmonic distortion (THD) [3], [4]. Many pulse width modulation (PWM) methods have been suggested to solve this issue by lowering harmonic distortion, thus enhancing the general GCPV performance.

Harmonic distortions in GCPVs can cause PQ problems, including voltage fluctuations, higher losses, and interference with other electrical devices [5]. Therefore, it is essential to implement effective PWM techniques to mitigate these effects and ensure the reliable operation of the system. Three well-known PWM techniques that have been extensively studied to reduce harmonic current distortion in GCPVs are sine PWM (SPWM), third harmonic injection PWM (THIPWM), and space vector PWM (SVPWM).

Numerous research efforts have been made to investigate various PWM techniques for inverters used in grid-connected photovoltaic (PV) systems, with the aim of improving power quality, mitigating harmonics, and optimizing system performance. Investigating the harmonic reduction potential of an SPWM inverter in a single-phase grid-connected PV system [6], while [7] discusses the design and analysis of GCPVs using various

PWM techniques for inverter control. The control of a two-level cascaded voltage source inverter for a GCPVs utilizing SVPWM and a quadratic boost converter was studied [8], highlighting the interplay between inverter control and converter topologies. A comparative analysis of PWM methods for a three-level NPC inverter was carried out [9], which contributed to the understanding of multilevel inverter control. A comprehensive review of PWM techniques in two-level voltage source inverters is presented, providing a current perspective and future directions in this area [10].

This study introduces a model for three-phase, single-stage GCPVs that incorporates SPWM, THIPWM, and SVPWM techniques. The aim is to minimize current harmonic distortion and enhance overall system efficiency. MATLAB Simulink is used to model the behavior of the system under various operating conditions to evaluate PWM methods for reducing harmonic distortions.

2. SYSTEM DESCRIPTION

The suggested GCPV model is illustrated in Figure 1 and is used to generate a power of 95.9 kW for simulation studies. The system configuration includes a PV array, a perturb and observe (P&O) maximum power point tracking (MPPT) algorithm, a DC link capacitor, a three-phase two-level (3Ph-2L) inverter, and a passive LCL filter connected to the grid.

2.1. Photovoltaic array model

The basic component of a photovoltaic system is a photovoltaic cell. It converts incident sunlight into corresponding electrical energy using the photovoltaic effect [11]. The single-diode PV cell model is widely used for the presentation of PV cells due to its simplicity. Figure 2 illustrates the equivalent circuit of the single diode PV cell model.

$$I_{pv} = I_{ph} - I_0 \left[e^{\frac{q(V_{pv}+I_{pv}R_s)}{(nKT)}} - 1 \right] - \left(V_{pv} + I_{pv}R_s \right)/R_{sh} \tag{1}$$
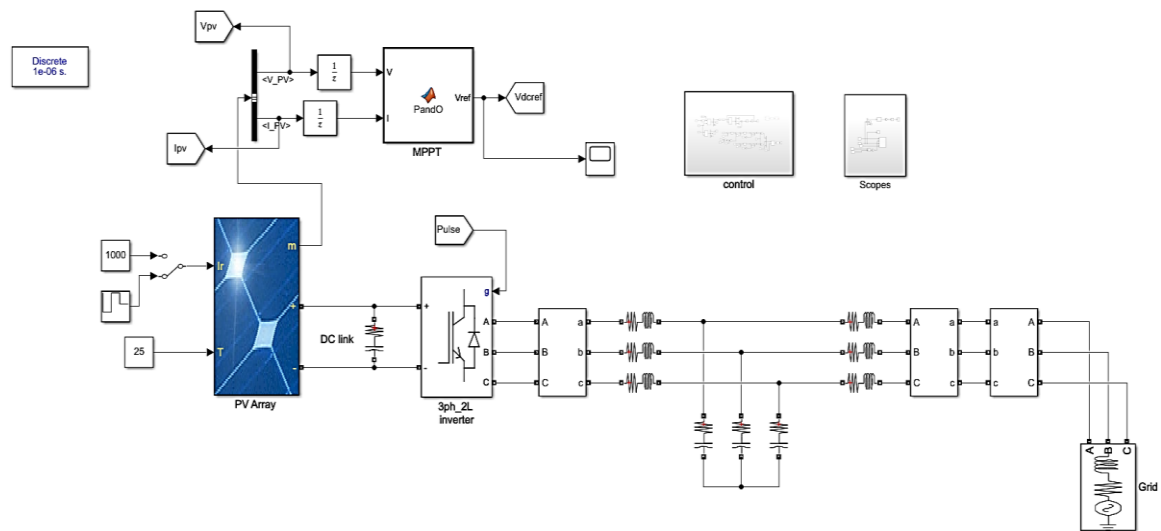

Figure 1. Configuration of a three-phase single-stage GCPVs
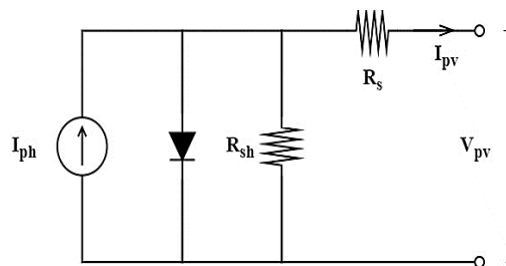

Figure 2. single-diode model of photovoltaic cell

In this context, I_{pv} represents the output current of the PV cell in (A), V_{pv} denotes the output voltage (V), I_{ph} denotes the photo-current in (A), I_o denotes the reverse saturation current in (A), R_{sh} represents the shunt resistance (Ω) , q is the electron charge (C), n is the diode ideality factor in the range 1 to 2, k represents the Boltzmann constant (J/K), and T represents the temperature of the PV cell in (K). The influence of solar radiation and the temperature of the PV cell on the current-voltage and power-voltage characteristics of the PV module is illustrated by Figures 3(a), 3(b), 4(a), and 4(b). These illustrations are based on the parameters provided in Table 1 of this study. A PV module consists of several PV cells arranged both in parallel and in series. The photovoltaic system in this study is made up of 18 parallel-connected strings, with each string containing 25 modules connected in series.
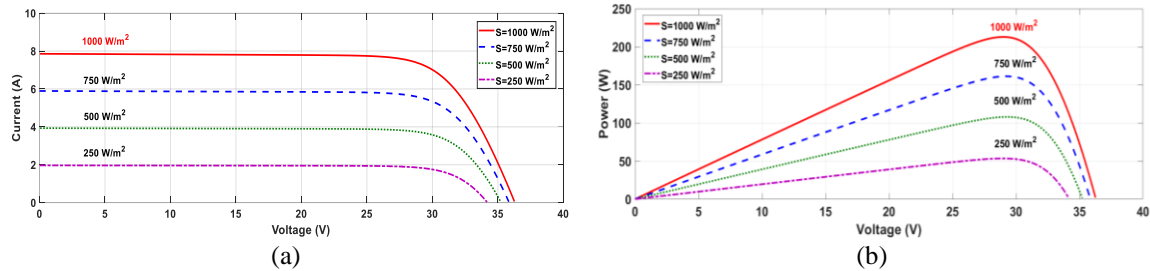

(a)   (b)

Figure 3. Solar irradiance effect with cell temp T = 25 °C: (a) I-V curve and (b) P-V curve

(a)   (b)
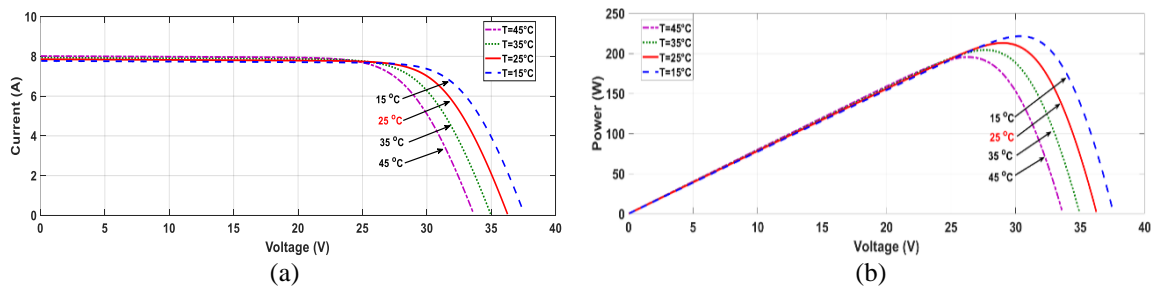
Figure 4. Cell temperature effect with solar irradiance S = 1000 W/m^2: (a) I-V curve and (b) P-V curve

Table 1. Electrical parameters for 1STH-215-P PV module

Specification	Value
Maximum power P	213.15 W
Open circuit voltage V_{oc}	36.3 V
Voltage at maximum power V_{mpp}	29 V
Short circuit current I_{sc}	7.84 A
Current at maximum power I_{mpp}	7.35
Open circuit voltage temperature coefficient	-0.36099 %/°C
Short circuit current temperature coefficient	0.102 %/°C

2.2. The perturb and observe algorithm (P&O)

An extensively applied MPPT technique in GCPVs is the P&O method [12]. The aim of this method is to continuously change the operation point up to the maximum power point (MPP) as environmental conditions change and thus improve the power output of the PV module [13]. Figure 5 illustrates the flowchart for the P&O algorithm. This approach involves continuously perturbing the voltage or current and monitoring the effects of these adjustments on the power output. The algorithm adjusts the operating point to increase power output by comparing the power output at the disturbed operating point with the previous power output. The voltage (V) and current (I) readings from the PV system serve as the algorithm's inputs in this case, and the reference voltage (Vref), which regulates the system's power converter, serves as the output [14].
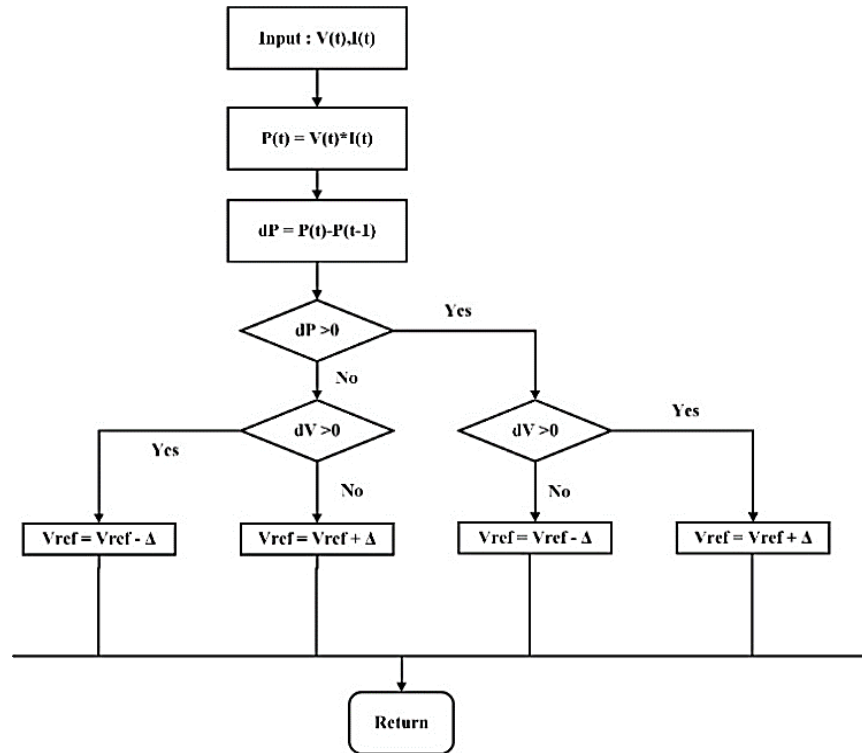
Figure 5. Flowchart of P&O MPPT algorithm

2.3. Three phase two-level (3Ph-2L) power inverter
2.3.1. Configuration and role

The 3Ph-2L inverter depicted in Figure 1 is composed of six power semiconductor switches, specifically insulated gate bipolar transistors (IGBTs), configured in three-phase bridge arms. Each of the arms encompasses two switches and two free-wheeling diodes set in an antiparallel arrangement with respect to the switches. The DC link capacitor C_{dc} to which the inverter is connected serves as an energy buffer and keeps the DC link voltage constant at the inverter input terminals. The PV system is connected to the intermediate circuit capacitor, where the direct current produced by the solar modules is received [15]. Usually employed at the inverter output, an LCL filter reduces high-frequency switching harmonic generation and improves output waveform quality during grid connection [16].

2.3.2. Control strategies inverters

Figure 6 depicts the proposed two-loop cascaded PI controller. Typically, the control system consists of two loops: an inner current control loop and an outer voltage control loop. With the aim of keeping the DC link voltage (Vdc) at the specified reference value (Vdcref), it is controlled by this external loop. The DC-link voltage error (Vdcref - Vdc) is fed to a PI controller, which generates the active current reference (Iref) for the inner current control loop, and the MPPT controller determines the voltage reference (Vdcref) based on this depending on the environmental conditions of the PV array to extract maximum power [17]. The Park transform is used to convert the three-phase voltages Vabc and currents Iabc from the natural ABC to the synchronous dq frame. This transformation is necessary for decoupling the active and reactive power components and simplifying the control process and involves the use of the line voltage angle (θ), which is typically obtained from a phase-locked loop synchronization block (PLL) [18]. The active and reactive currents Id and Iq in the dq frame are controlled by the inner control. The outer voltage control loop provides the active current reference Idref. For unity power factor operation, the reactive current reference Iqref is usually set to zero [19]. The current errors (Idref-Id) and (Iqref-IIq) are fed to separate PI controllers, which generate the respective voltage references (Vdref and Vqref) in the dq frame. Using the inverse Park transform, the voltage references (Vdref and Vqref) in the dq frame are reset to the natural ABC frame, generating the three-phase voltage references for Vabcref. These voltage references are adopted as inputs to the PWM block that generates the switching signals for the 3Ph-2L inverter.

2.4. PWM technique

PWM is extensively utilized in power converters such as three-phase, two-level inverters. Power electronic devices are switched at high frequencies to produce a modulated signal, which is then filtered to obtain the desired AC output [20].

2.4.1. SPWM technique

The primary goal of the SPWM technique in GCPVs is to transform the solar panel's direct current (DC) into alternating current (AC) suitable for feeding into the electrical grid [21], [22]. Figure 7 illustrates the operation of SPWM by comparing a high-frequency triangular carrier signal with a sinusoidal reference signal, so depicting the intended output voltage [23]. As the reference signal surpasses the carrier wave, the associated switch in the inverter is activated, and when the reference signal drops below the carrier wave, the switch is deactivated. This process produces a series of pulses with different widths for each phase, effectively producing an output waveform that is close to the sinusoidal reference signal [24], [25].

The three sinusoidal reference waveforms proposed in the present model (Vref$_{Sa}$, Vref$_{Sb}$, Vref$_{Sc}$) represent the desired output voltage for each phase abc, with each phase shifted by 120 degrees, and are given by (2).

$$V_{ref_{Sa}} = \sin(\omega t)$$
$$V_{ref_{Sb}} = \sin\left(\omega t - \frac{2\pi}{3}\right)$$
$$V_{ref_{Sc}} = \sin\left(\omega t + \frac{2\pi}{3}\right)$$
(2)

Where: ω denotes the angular frequency of the output voltage and t represents time.
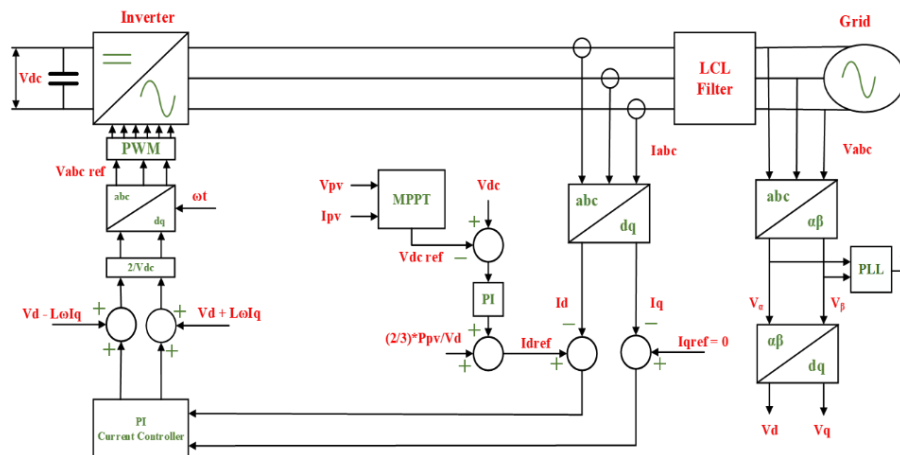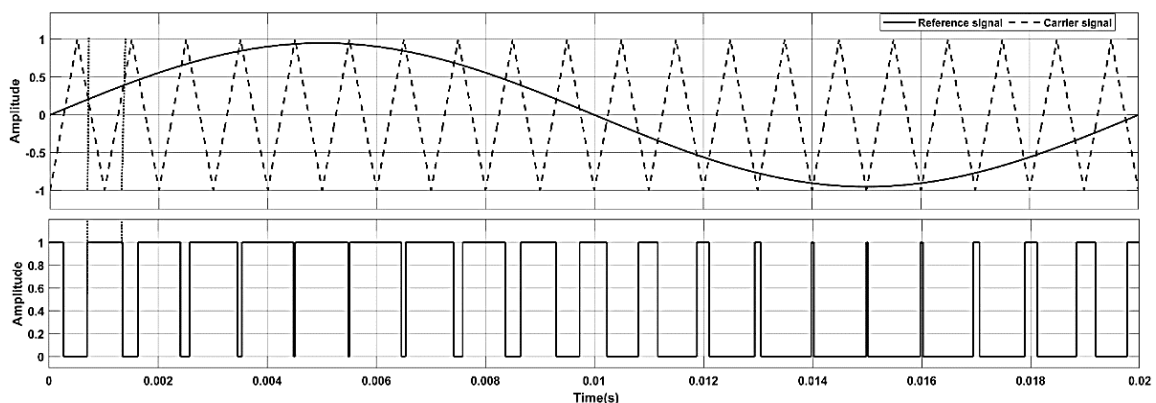

Figure 6. Control block diagram

Figure 7. The function principle of SPWM

2.4.2. Third harmonic injected PWM

Figure 8 depicts the principal function of the THIPWM technique. In this approach, two sine waveforms are merged to create a reference signal, with one sine wave selected to have a frequency three times greater than the other. Subsequently, trigger pulse signals are generated by comparing the reference waveform with the carrier signal. The THI reference signal evaluates the magnitude of the third harmonic component to verify the desired output quality. This technique, along with the flattened structure of the reference signal, minimizes switching losses. By eliminating third harmonic components, this approach enables more effective utilization of DC sources [26]. The THI reference signal described in (3) is created by combining the reference sine wave with a third harmonic signal attenuated by $\frac{1}{3\sqrt{3}}$. This method results in a 15% enhancement of the sine wave's fundamental component.
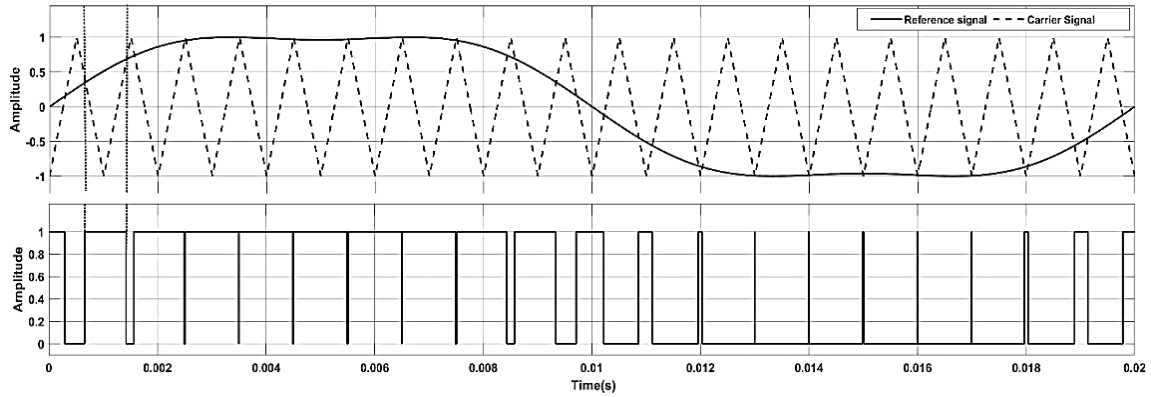

Figure 8. The function principle of THIPWM

The equation for the three reference waveforms with the third harmonic component injected can be expressed as (3) [27], [28].

$$
\left.\begin{aligned}
V_{ref_{THIa}} &= \frac{2}{\sqrt{3}}\sin(\omega t) + \frac{1}{3\sqrt{3}}\sin(3\omega t) \\
V_{ref_{THIb}} &= \frac{2}{\sqrt{3}}\sin(\omega t - 2\pi/3) + \frac{1}{3\sqrt{3}}\sin(3\omega t) \\
V_{ref_{THIc}} &= \frac{2}{\sqrt{3}}\sin(\omega t + 2\pi/3) + \frac{1}{3\sqrt{3}}\sin(3\omega t)
\end{aligned}\right\}
\tag{3}
$$

Where ω is the output voltage's angular frequency and t denote time.

2.4.3. Space vector PWM

SVPWM is an advanced technique for controlling three-phase, two-level inverters by optimizing switching states to minimize harmonic distortion and improve output voltage quality. It effectively utilizes the available voltage space vectors to generate a desired output voltage to improve the performance of motor drives and power converters. To begin implementing SVPWM, it is necessary to determine the vector of reference voltage $\overline{V}r$ in the α–β stationary frame, utilizing the standard Clarke transform as described in (4) [27], [29].

$$
\begin{bmatrix} V_{r\alpha} \\ V_{r\beta} \end{bmatrix} = \frac{2}{3} \begin{bmatrix} 1 & -\frac{1}{2} & -\frac{1}{2} \\ 0 & \frac{\sqrt{3}}{2} & -\frac{\sqrt{3}}{2} \end{bmatrix} \begin{bmatrix} V_a \\ V_b \\ V_c \end{bmatrix}
\tag{4}
$$

V_a, V_b, and V_c are the three coordinate reference voltages. Additionally, the vector $\overline{V}_r$ can be expressed in the following complex form, as (5).

$$
\overline{V}_r = V_{r\alpha} + jV_{r\beta}
\tag{5}
$$

Consequently, the magnitude $|V_r|$ and the phase θ of $\overline{V}_r$ can be determined as (6).

$$\begin{cases} |V_r| = \sqrt{V_{r\alpha}^2 + V_{r\beta}^2} \\ \theta = tan^{-1}\left(\frac{V_{r\alpha}}{V_{r\beta}}\right) \end{cases} \tag{6}$$

Due to the complementary commutation of the upper and lower switches, either the upper or lower arm switch status can be represented. The switches are marked "1" for ON and "0" for OFF. Six active vectors and two zero vectors represent the eight potential switching states of the inverter. Table 2 displays the various reference voltages corresponding to each of these eight states.

In Figure 9(a), the hexagonal diagram displays active voltages ($V_1 - V_6$) along its axes, while the two zero vectors ($V_0 - V_7$) represent zero voltage applications. The SVPWM method uses these eight switching configurations to estimate the reference voltage vector V_r. For the purpose of illustration, assume that the sector1 contains the reference vector, as shown in Figure 9(a). V_1 and V_2 are the two voltage vectors closest to the reference vector, and V_0 or V_7 is the zero-voltage vector. T_1, T_2, and T_0 represent the respective application times for the reference vectors. Allocating these vectors during a switching period considers the following restrictions, as shown in Figure 9(b).

- In a single switching period, the power semiconductors should not switch between their ON and OFF states more than twice.
- The voltage at neutral point should be kept close to zero.

The volt-second equation is utilized to determine the application times and is expressed as (7).

$$\begin{cases} T_s.\overline{V_r} = T_1.\overline{V_1} + T_2.\overline{V_2} + \overline{T_0}.\overline{V_0} \\ T_s = T_1 + T_2 + T_0 \end{cases} \tag{7}$$

T_s is the sampling time in this case. By employing the space vector diagram and (7), we can express as (8).

$$\begin{cases} T_s|V_r|cos\theta = T_1|V_1| + T_2|V_2|cos60° \\ T_s|V_r|sin\theta = T_2|V_2|sin60° \end{cases} \tag{8}$$

Table 2. Switch states and output vectors

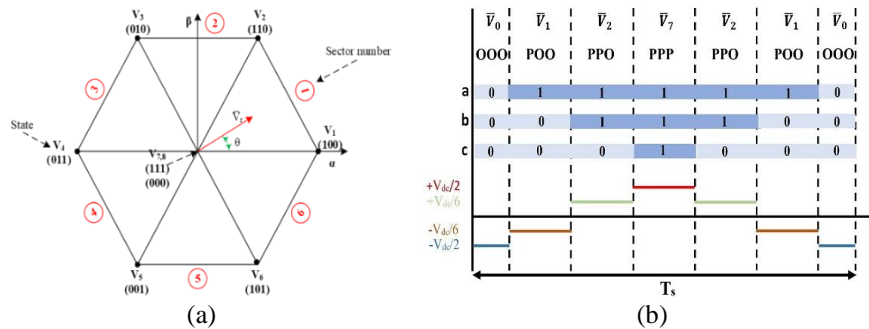| Space vector	V_{an}	V_{bn}	V_{cn}	$|V_r|$	θ
$V_0(000)$	0	0	0	0	0°
$V_1(100)$	$\frac{2}{3}V_{dc}$	$\frac{-1}{3}V_{dc}$	$\frac{-1}{3}V_{dc}$	V_{dc}	0°
$V_2(110)$	$\frac{1}{3}V_{dc}$	$\frac{-1}{3}V_{dc}$	$\frac{-2}{3}V_{dc}$	V_{dc}	60°
$V_3(010)$	$\frac{-1}{3}V_{dc}$	$\frac{2}{3}V_{dc}$	$\frac{1}{3}V_{dc}$	V_{dc}	120°
$V_4(011)$	$\frac{-2}{3}V_{dc}$	$\frac{1}{3}V_{dc}$	$\frac{1}{3}V_{dc}$	V_{dc}	180°
$V_5(001)$	$\frac{-1}{3}V_{dc}$	$\frac{-1}{3}V_{dc}$	$\frac{2}{3}V_{dc}$	V_{dc}	240°
$V_6(101)$	$\frac{1}{3}V_{dc}$	$\frac{-2}{3}V_{dc}$	$\frac{1}{3}V_{dc}$	V_{dc}	300°
$V_7(111)$	0	0	0	0	0°

Figure 9. 2L-SVPWM pattern: (a) vector diagram and sectors numbering and (b) switching states

These application times can be found by solving (8).

$$\begin{cases} T_1 = \frac{\sqrt{3}}{V_{dc}} |V_r| T_s \sin(\frac{\pi}{3} - \theta) \\ T_2 = \frac{\sqrt{3}}{V_{dc}} |V_r| T_s \sin(\theta) \\ T_0 = 1 - (T_1 + T_2) \end{cases} \tag{9}$$

For the two-level inverter shown in Figure 1, the general expressions for the application times are derived by applying this principle to the six operating sectors, as in (10).

$$\begin{cases} T_1 = \frac{\sqrt{3}}{V_{dc}} |V_r| T_s \sin(k_{sn} \frac{\pi}{3} - \theta) \\ T_2 = \frac{\sqrt{3}}{V_{dc}} |V_r| T_s \sin\left(\theta - (k_{sn} - 1)\frac{\pi}{3}\right) \\ T_0 = 1 - (T_1 + T_2) \end{cases} \tag{10}$$

Where, k_{sn} represents the sector number. The switching sequences for all operating ranges are listed in Table 3.

Table 3. Conventional SVPWM vector sequence

Sector N°	Switching sequence
1	V0_V1_V2_V7_V2_V1_V0
2	V0_V3_V2_V7_V2_V3_V0
3	V0_V3_V4_V7_V4_V3_V0
4	V0_V5_V4_V7_V4_V5_V0
5	V0_V5_V6_V7_V6_V5_V0
6	V0_V1_V6_V7_V6_V1_V0

3. RESULTS AND DISCUSSION

This section is devoted to assessing the performance of the suggested PWM and summarizes the key findings of the study. For this purpose, analyses of the THD current fed in under different operating conditions and comparisons with SPWM, THIPWM, and SVPWM are carried out for grid-connected operation. The proposed PWM techniques are evaluated under rapidly changing irradiance conditions. To implement the proposed model shown in Figure 1, the MATLAB/Simulink software package was used. The values considered for the simulation are listed in Table 4. The level of irradiation determines the output power of a PV system and thus the current that flows through the inverter. As irradiance increases, the current increases, potentially affecting harmonic content and THD.

The irradiance profile depicted in Figure 10 illustrates an initial irradiance of 550 W/m^2 from 0 to 0.5 seconds, followed by an abrupt increase to 1000 W/m^2 at 0.5 s, and a subsequent decrease to 750 W/m^2 at 1 s, continuing until 1.5 s. Throughout the simulation, the temperature remains constant at 25 °C. Figures 11, 12, and 13 present the grid current waveform and its corresponding harmonic spectrum for SPWM, THIPWM, and SVPWM, respectively, at three distinct irradiance levels.

Table 4. Specifications values for the proposed model

Specifications	Value
Rated power of PV array (P_{pv})	95.92 Kw
PV array open-circuit voltage of the (V_{oc})	907.6 V
DC-link capacitor (C_{dc})	1000 µF
Frequency switch f_{sw}	10 Khz
Inverter side inductor in LCL filter (L_i)	500 µH
Capacitor in LCL filter (C_i)	100 µF
Grid side inductor in LCL filter (L_g)	500 µH
Grid voltage (V_{LL})	400 V
Grid frequency (f_g)	50 Hz

Using the SPWM technique, Figure 11 illustrates how the inverter current responds to changes in solar radiation. It has THD values of 2.48%, 1.20%, and 1.72% at irradiances of 550 W/m^2, 1000 W/m^2, and 750 W/m^2, respectively. Figure 12 shows the response of the inverter current under varying solar irradiance with the THIPWM technique and shows improved performance compared to the SPWM. The THD values for

THIPWM are lower than those of SPWM at all irradiances, with THD values of 2.30%, 0.93%, and 1.36% at 550 W/m², 1000 W/m², and 750 W/m². The lowest THD of 0.93% is achieved at the standard test condition of 1000 W/m².

Figure 13 shows the inverter current response to varying solar irradiance using SVPWM, illustrating the lowest THD values among the three techniques across all irradiance levels. At 1000 W/m2, SVPWM achieves the lowest THD of 0.78%, outperforming both SPWM and THIPWM. The THD values for SVPWM are 1.94%, 0.78%, and 1.36% at irradiances of 550 W/m², 1000 W/m², and 750 W/m², respectively.
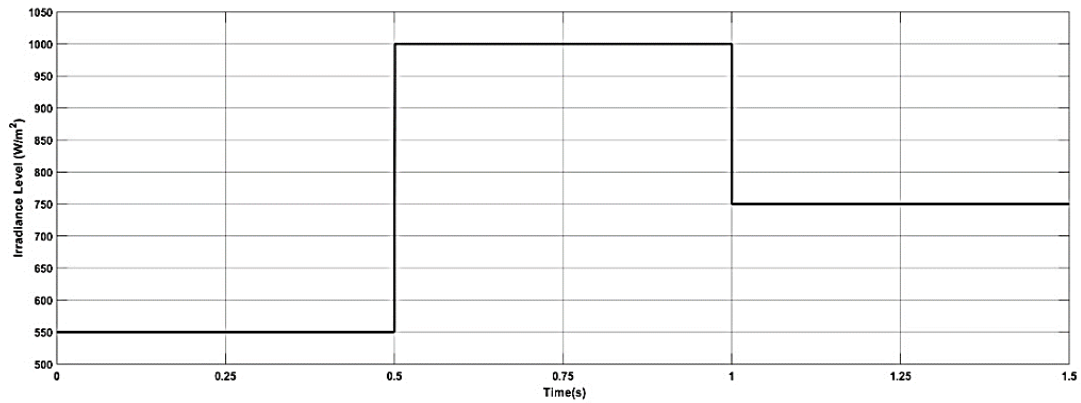
Figure 10. Irradiance scenario conditions
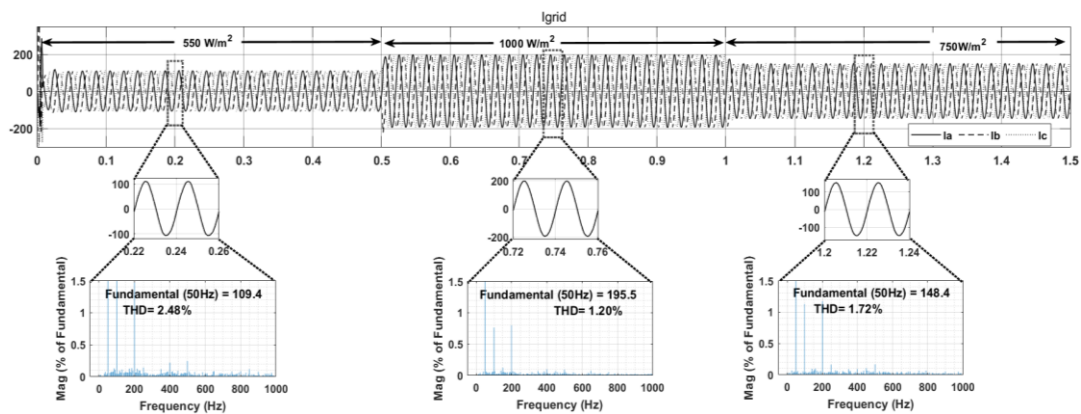
Figure 11. Current I_a injected to the grid using SPWM at varying irradiance conditions
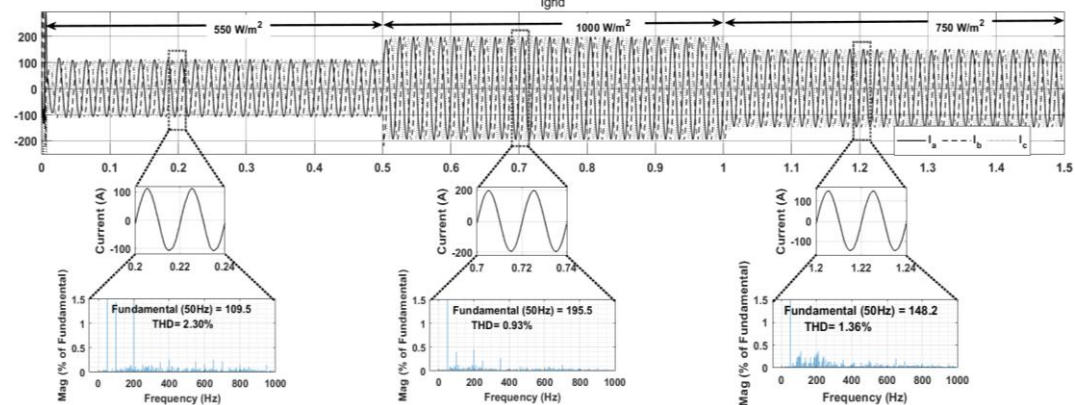
Figure 12. Current I_a injected to the grid using THIPWM at varying irradiance conditions
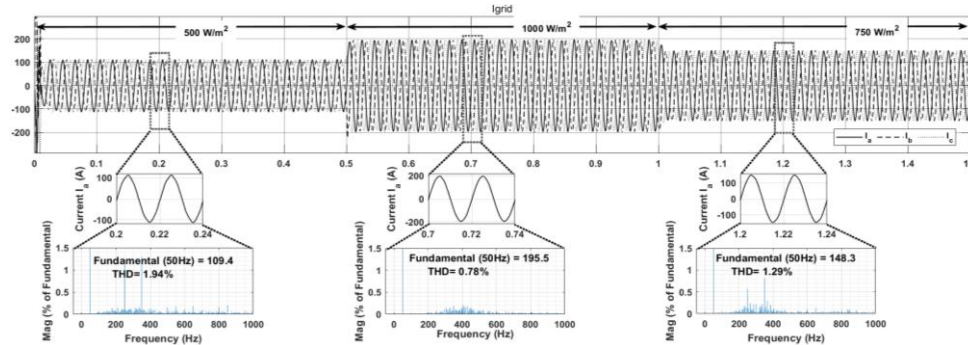
Figure 13. Current I$_a$ injected to the grid using SVPWM at varying irradiance conditions

4. CONCLUSION

The study shows that implementing advanced PWM techniques, particularly SVPWM in three-phase single-stage GCPVs, can significantly reduce the THD current supplied to the grid. The SVPWM technique proves to be the most effective method for mitigating harmonic distortion and achieves the lowest THD values across all simulated irradiances. These results highlight the importance of using appropriate PWM techniques in the design of photovoltaic systems to improve power quality and comply with grid connection standards.

REFERENCES

[1]   Z. Ben Mahmoud and A. Khedher, "A comprehensive review on space vector based-PWM techniques for common mode voltage mitigation in photovoltaic multi-level inverters," *Energies (Basel)*, vol. 17, no. 4, p. 916, Feb. 2024, doi: 10.3390/en17040916.
[2]   A. M. Mahfuz-Ur-Rahman, Md. R. Islam, K. M. Muttaqi, Md. A. Rahman, and D. Sutanto, "An advanced modulation technique for transformer less grid connected inverter circuits used in solar photovoltaic systems," *IEEE Transactions on Industrial Electronics*, vol. 70, no. 4, pp. 3878–3887, Apr. 2023, doi: 10.1109/TIE.2022.3177805.
[3]   N. Anang and W. M. W. Muda, "Analysis of total harmonic distortion in single-phase single-stage grid-connected photovoltaic system," *International Journal of Power Electronics and Drive Systems (IJPEDS)*, vol. 14, no. 1, p. 471, Mar. 2023, doi: 10.11591/ijpeds.v14.i1.pp471-479.
[4]   W. A. A. Salem, W. G. Ibrahim, A. M. Abdelsadek, and A. A. Nafeh, "Grid connected photovoltaic system impression on power quality of low voltage distribution system," *Cogent Engineering*, vol. 9, no. 1, Dec. 2022, doi: 10.1080/23311916.2022.2044576.
[5]   A. R. Ali, R. K. Antar, and A. G. A. Abdulghafoor, "Harmonics mitigation technique for asymmetrical multilevel inverter fed by photovoltaic sources," *Bulletin of Electrical Engineering and Informatics*, vol. 13, no. 2, pp. 865–873, Apr. 2024, doi: 10.11591/eei.v13i2.6607.
[6]   S. K. Dalai, R. Sahu, and C. S. Tripathy, "Harmonic mitigation in single-phase grid connected photovoltaic system using SPWM inverter," in *2020 International Conference on Computational Intelligence for Smart Power System and Sustainable Energy (CISPSSE)*, IEEE, Jul. 2020, pp. 1–6, doi: 10.1109/CISPSSE49931.2020.9212280.
[7]   S. A. Ravindra, S. M. Ravindra, and K. K. More, "Design and analysis of grid-connected photo-voltaic system by using different PWM techniques for inverter control," in *2020 IEEE PES/IAS Power Africa*, IEEE, Aug. 2020, pp. 1–4, doi: 10.1109/PowerAfrica49420.2020.9219922.
[8]   S. M. Basha and Dr. K. Nagaraju, "Controlling of Cascaded Voltage Source Two Level Inverter Based Grid Connected PV system by using SVPWM and quadratic boost converter," *International Journal of Electrical and Electronics Research*, vol. 10, no. 3, pp. 716–721, Sep. 2022, doi: 10.37391/ijeer.100349.
[9]   M. Deenakonda, V. V. V. Inti, G. R. Swamy, M. Lavanya, P. Bhavani, and B. T. Rao, "Comparative Analysis of PWM methods for three level neutral point clamped inverter," in *Lecture Notes of the Institute for Computer Sciences, Social-Informatics and Telecommunications Engineering, LNICST*, vol. 537, 2024, pp. 86–95, doi: 10.1007/978-3-031-48891-7_7.
[10] D. Chattejee, C. Chakraborty, and S. Dalapati, "Pulse-width modulation techniques in two-level voltage source inverters – state of the art and future perspectives," *Power Electronics and Drives*, vol. 8, no. 1, pp. 335–367, Jan. 2023, doi: 10.2478/pead-2023-0023.
[11] D. Toumi *et al.*, "Maximum power point tracking of photovoltaic array using fuzzy logic control," *International Journal of Power Electronics and Drive Systems (IJPEDS)*, vol. 13, no. 4, p. 2440, Dec. 2022, doi: 10.11591/ijpeds.v13.i4.pp2440-2449.
[12] R. N. Hasanah, F. Yuniar, O. Setyawati, H. Suyono, D. R. Sawitri, and T. Taufik, "A modified perturb-and-observe control for improved maximum power point tracking performance on grid-connected photovoltaic system," *International Journal of Technology*, vol. 15, no. 1, p. 99, Jan. 2024, doi: 10.14716/ijtech.v15i1.5316.
[13] R. D. A. Raj and K. A. Naik, "Priority queue-based switching matrix algorithm for adaptive neuro-fuzzy inference system assisted MPPT controlled PV system," *Energy Conversion and Management*, vol. 293, p. 117519, Oct. 2023, doi: 10.1016/j.enconman.2023.117519.
[14] M. Abu-Zaher, Y. Atia, F. K. Abo-Elyousr, and E. El-Zohri, "Experimental realization for P&O maximum power point tracking applied for single-stage three-phase grid-connected photovoltaic system," in *2019 21st International Middle East Power Systems Conference (MEPCON)*, IEEE, Dec. 2019, pp. 704–709, doi: 10.1109/MEPCON47431.2019.9008070.
[15] R. Rudraram, S. Chinnathambi, and M. Mani, "A novel intelligent neural network techniques of UPQC with integrated solar PV system for power quality enhancement," *International Journal of Electronics and Telecommunications*, pp. 605–613, Jun. 2023, doi: 10.24425/ijet.2023.146514.
[16] T. Zhu *et al.*, "Analysis and suppression of harmonic resonance in photovoltaic grid-connected systems," *Energies (Basel)*, vol. 17, no. 5, p. 1218, Mar. 2024, doi: 10.3390/en17051218.
[17] A. I. M. Ali and H. R. A. Mohamed, "Improved P&O MPPT algorithm with efficient open-circuit voltage estimation for two-stage grid-integrated PV system under realistic solar radiation," *International Journal of Electrical Power & Energy Systems*, vol. 137, p. 107805, May 2022, doi: 10.1016/j.ijepes.2021.107805.

[18] M. E. Ahmad, Ali. H. Numan, and D. Y. Mahmood, "Enhancing performance of grid-connected photovoltaic systems based on three-phase five-level cascaded inverter," *International Journal of Power Electronics and Drive Systems (IJPEDS)*, vol. 12, no. 4, p. 2295, Dec. 2021, doi: 10.11591/ijpeds.v12.i4.pp2295-2304.

[19] A. S. Chatterjee, "A bus clamping PWM-based improved control of grid tied PV inverter with LCL filter under varying grid frequency condition," *IETE Journal of Research*, vol. 69, no. 2, pp. 862–878, Feb. 2023, doi: 10.1080/03772063.2020.1844067.

[20] R. Aboo Faris, M. S. Rajendran, and V. P. Suresh, "Performance analysis of modulation techniques for three-phase high-frequency VSC," in *2023 IEEE 20th India Council International Conference (INDICON)*, IEEE, Dec. 2023, pp. 1068–1075, doi: 10.1109/INDICON59947.2023.10440962.

[21] E. Jaoide, F. El Aamri, M. Outazkrit, A. Radouane, and A. Mouhsen, "Maximum power point tracking and space vector modulation control of quasi-z-source inverter for grid-connected photovoltaic systems," *International Journal of Electrical and Computer Engineering (IJECE)*, vol. 14, no. 2, p. 1424, Apr. 2024, doi: 10.11591/ijece.v14i2.pp1424-1436.

[22] S. Xu, R. Shao, B. Cao, and L. Chang, "Single-phase grid-connected PV system with golden section search-based MPPT algorithm," *Chinese Journal of Electrical Engineering*, vol. 7, no. 4, pp. 25–36, Dec. 2021, doi: 10.23919/CJEE.2021.000035.

[23] Y. I. Sysoeva and S. N. Shelyug, "Analysis of PWM method for TFC (3L-NPC)," in *2023 Belarusian-Ural-Siberian Smart Energy Conference (BUSSEC)*, IEEE, Sep. 2023, pp. 127–131, doi: 10.1109/BUSSEC59406.2023.10296440.

[24] M. Saini *et al.*, "Improvement of power quality of a 200 kW grid-connected PV system," *International Journal of Power Electronics and Drive Systems (IJPEDS)*, vol. 14, no. 3, p. 1759, Sep. 2023, doi: 10.11591/ijpeds.v14.i3.pp1759-1767.

[25] W. Zhe, D. Ishak, and M. Hamidi, "a grid-connected inverter with grid-voltage-weighted feedforward control based on the quasi-proportional resonance controller for suppressing grid voltage disturbances," *Energies (Basel)*, vol. 17, no. 4, p. 885, Feb. 2024, doi: 10.3390/en17040885.

[26] C. S. Yee, S. A. Azmi, L. J. Hwai, M. F. N. Tajuddin, M. Z. A. Zahari, and S. R. A. Rahim, "Comparative evaluation of three-phase inverter topologies based on voltage boosting features," *Journal of Physics: Conference Series*, vol. 2641, no. 1, p. 012021, Nov. 2023, doi: 10.1088/1742-6596/2641/1/012021.

[27] F. Fatima and B. Nourddine, "Harmonic elimination by SPWM and THIPWM techniques applied in photovoltaic inverters," *International Journal of Applied Power Engineering (IJAPE)*, vol. 10, no. 2, p. 159, Jun. 2021, doi: 10.11591/ijape.v10i2.pp159-172.

[28] O. E. Ozciflikci and M. Koc, "Comparison of interior mounted permanent magnet synchronous motor drives with sinusoidal, third harmonic injection, and space vector pulse width modulation strategies with particular attention to current distortions and torque ripples," *Electrica*, Oct. 2022, doi: 10.5152/electrica.2022.22035.

[29] M. B. Sadr, D. A. Khaburi, M. Jamei, and H. Radmanesh, "Implementation and analysis of SVM modulation method in linear and over-modulation zones," in *2022 13th Power Electronics, Drive Systems, and Technologies Conference (PEDSTC)*, IEEE, Feb. 2022, pp. 630–634, doi: 10.1109/PEDSTC53976.2022.9767234.

BIOGRAPHIES OF AUTHORS

Bouledroua Adel was born in Annaba (Algeria), on March 4, 1982. He graduated the University of Badji Mokhtar, Department of Electromechanical Engineering (Algeria), in 2005. He received the degree of Magister in electromechanical Engineering from the University of Badji Mokhtar Annaba in 2008, and he is currently pursuing his Ph.D. from Badji Mokhtar University. His research interests include the field of renewable energy, photovoltaic power system, wind application, power electronics, motor drives, and artificial intelligence. He can be contacted at email: adel.bouledroua@univ-annaba.dz.
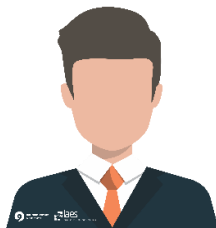
Mesbah Tarek received his B.E. degree, Master and Ph.D. Degrees in Electrical Engineering from Badji Mokhtar University of Annaba, Algeria. Currently he is a professor in the Badji Mokhtar University of Annaba. His research interests include the field of power grid, smart grid, power system optimization, and renewable energy. He can be contacted at email: tarek.mesbah@univ-annaba.dz.
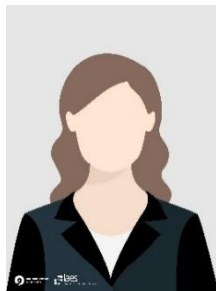
Kelaiaia Samia received her B.E. degree, Master and Ph.D. Degree in Electrical Engineering from Badji Mokhtar University of Annaba, Algeria. Currently she is an assistant professor with the Badji Mokhtar University of Annaba. Her current research interests include power electronics, renewable energy, and renewable energy integration to power grid. She can be contacted at email: samia.kelaiaia@univ-annaba.dz.